Thermal-electromechanical Modeling of Magnetically Levitated Rotors under Vacuum Conditions

Antje Deckert*
Astro- und Feinwerktechnik Adlershof GmbH
Berlin, Germany

Abstract

This paper introduces a possibility to couple the thermal analyses of a magnetically levitated rotor, which is driven under vacuum condition, with models of its electromechanical loop. By means of this coupling, effects can be represented that are not visible when considering the thermal behavior and the electromechanical loop separately. The models have been parameterized for a huge number of geometrical and physical properties. The derived algorithms are implemented in MATLAB and accessible via the graphical user interface "MagBeS – Magnetic Bearing Simulator". This makes the algorithm applicable for different users and varying systems. Analyses are presented that demonstrate the interaction of the thermal and electromechanical behavior and it is shown that additional potentially critical operating modes can be identified. Furthermore, a novel approach for the experimental determination of the occurring rotor losses by means of temperature measurements and thermal analyses is presented.

1 Introduction

Active magnetic suspension of rotating machinery provides some main advantages over conventional bearing technologies considering lifetime, mechanical wear, microvibrations and controllability. However, the physical coupling effects of such mechatronic system make it rather complex. Of course, tools providing advanced (e. g. finite element) analyses of the single physical domains are state of the art and also multiphysics software has been established during the last few years. Nonetheless, implementing these models is time-consuming and requires a rather good knowledge of the geometry of the system. The design approaches for magnetic bearings found in literature mostly concentrate on a single physical domain, where the other influencing factors are considered as black boxes or simple linear systems. Furthermore, the temperature of the magnetically levitated rotor mainly influences its behavior. All these aspects yield the conclusion that it is quite obvious to implement multiphysical models of such systems.

Most of the models used for simulating magnetically levitated Rotors are feasible for the analysis of the electromechanical circuit, e. g. [1, 2, 3, 4, 5]. Thermal investigations of such systems are limited to simplified analyses using thermal networks, e. g. [6, 7]. The temperature influence on the mechanical, electrical and magnetic properties and the coupling between electromechanical circuit and thermal behavior have not yet been discussed quantitavely or considered and analyzed in a coupled model. By means of the coupling, effects can be made visible that cannot be identified when applying separate analysis of the thermal and electromechanical behavior.

The paper includes a short introduction of the used models of the rotordynamics, the magnetic bearing, the control loop, and the thermal behavior. The numerical coupling is described afterwards. The application of the developed algorithm is shown exemplarily using a transient analysis and a novel approach for determine the occurring bearing losses by temperature measurements and thermal modeling.

*a.deckert@astrofein.com, Albert-Einstein-Strasse 12, Phone: +49-30-63 92-10 56, Fax: +49-30-63 92-10 02

2 Domain Specific Models

The considered couplings are shown in figure 1. The main extension when compared to previous works is the inclusion of the thermal analyses. In the following, the domain specific models and algorithms are presented.

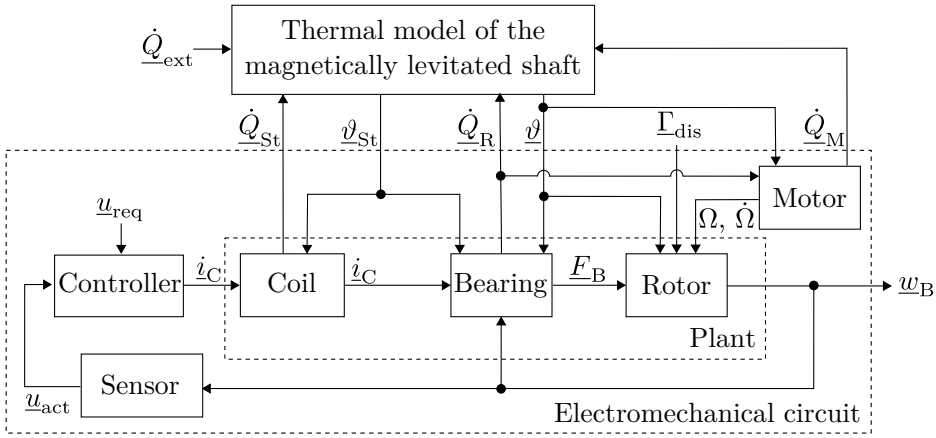

Legend

$\underline{\Gamma}_{\mathrm{dis}}$... Disturbance forces/torques
$\underline{F}_{\mathrm{B}}$... Bearing forces
Ω... Rotor speed
$\underline{w}_{\mathrm{L}}$... Rotor displacement within the bearings
$\underline{u}_{\mathrm{req}}, \underline{u}_{\mathrm{act}}$... Required and actual voltage, respectively
$\underline{i}_{\mathrm{C}}$... Control current

$\underline{\dot{Q}}_{\mathrm{ext}}$... External heat sources
$\underline{\dot{Q}}_{\mathrm{St}}$... Stator heat sources within bearing
$\underline{\dot{Q}}_{\mathrm{R}}$...Rotor heat sources within bearing
$\underline{\dot{Q}}_{\mathrm{M}}$... Motor heat sources
$\underline{\vartheta}$... Rotor temperatures
$\underline{\vartheta}_{\mathrm{St}}$... Stator temperatures

Figure 1: Block diagram of the magnetically levitated shaft

2.1 Rotordynamics

Within the scope of this study, it is assumed that the elastic shaft of the magnetically levitated system can be analysed via a limited number of shaft elements ($N < 20$). Hence, a multiple disc rotor model has been chosen and the following assumptions are applied:

- the shaft is suspended by two radial magnetic bearings,
- the shaft is torsion resistant,
- no disturbances occur in axial direction,
- the motor does only yield a torque about the axial axis,
- the bearing forces act on a discrete point, and
- the rotor discs are stiff.

The shaft rotating with a frequency Ω yields a second order differential system of equation:

$$\mathbf{M}\underline{\ddot{\kappa}} + (\mathbf{D} + \mathbf{G}\Omega)\,\underline{\dot{\kappa}} + \left(\mathbf{K} + \mathbf{G}\dot{\Omega}\right)\underline{\kappa} = \underline{\Gamma}_{\mathrm{dis}}. \tag{1}$$

The system matrices **M**, **D** and **K** contain the mass, damping and stiffness properties. **G** is the gyroscopic stiffness matrix. The vector $\underline{\kappa}$ represents the generalized coordinates. External disturbance

torques and forces are contained in the generalized force vector $\underline{\Gamma}_{\mathrm{dis}}$. The latter can be used for inclusion of the bearing forces. For frequency domain analyses, linear models are required. Hence, in this case, the bearing forces are included via linear force characteristics, $\mathbf{K}_{\mathrm{B}}$ for the force-displacement factor and $\mathbf{K}_i$ for the force-current factor. For a shaft suspended by two radial magnetic bearings (B1 and B2), the equation of motions can be written as

$$\underbrace{\begin{bmatrix}\mathbf{M}_{\mathrm{B1}} & \mathbf{0}\\ \mathbf{0} & \mathbf{M}_{\mathrm{B2}}\end{bmatrix}}_{\mathbf{M}_{\mathrm{B}}}\begin{pmatrix}\ddot{\underline{w}}_{\mathrm{B1}}\\ \ddot{\underline{w}}_{\mathrm{B2}}\end{pmatrix}-\underbrace{\begin{bmatrix}\mathbf{K}_{\mathrm{B1}} & \mathbf{0}\\ \mathbf{0} & \mathbf{K}_{\mathrm{B2}}\end{bmatrix}}_{\mathbf{K}_{\mathrm{B}}}\begin{pmatrix}\underline{w}_{\mathrm{B1}}\\ \underline{w}_{\mathrm{B2}}\end{pmatrix}-\underbrace{\begin{bmatrix}\mathbf{K}_{i1} & \mathbf{0}\\ \mathbf{0} & \mathbf{K}_{i2}\end{bmatrix}}_{\mathbf{K}_i}\begin{pmatrix}\underline{i}_{\mathrm{St1}}\\ \underline{i}_{\mathrm{St2}}\end{pmatrix}=-\begin{pmatrix}\underline{F}_{\mathrm{B1}}\\ \underline{F}_{\mathrm{B2}}\end{pmatrix}. \tag{2}$$

2.2 Electromagnetic Models

The analytical and numerical calculation of electromagnetic fields is discussed in various publications, e. g. [8, 9, 10, 11, 12]. The resulting approaches for determination of the forces and losses of magnetic bearings can also be found numerously in literature, e. g. [3, 13, 14, 5]. These approaches vary from linearized analytical equations to 3D finite element simulations. Analytical models, especially linearized equations, are often used for first estimations and rotordynamic or control loop analyses, e. g. [15, 16]. Furthermore, they serve as a basis for design and optimization approaches [17, 18]. Nonetheless, most of these models neglect stray fields and saturation of the magnetic field. Including these effects make the analytical models rather complex [2, 19].

Alternatively, magnetic bearings can be simulated numerically by using finite element programs. Commercial software yields the main advantage that they are mostly feasible for 3D modeling and that a huge number of analyses is already included in these packages, e. g. QuickField™, Maxwell® und Flux® [20, 21, 22]. However, they are rather expensive. Freeware is either limited to the dimensions (FEMM [23]) or nodes (student's version of QuickField™ [24]). Nonetheless, it might yield a good compromise between the simplified analytical models and the costs of the commercial finite element software. Within the scope of this study, the finite element software FEMM (Finite Element Method Magnetics, Version 4.2) has been used for electromagnetic field computations.

FEMM bases on the numerical solution of the *Maxwell* equations for the magnetic vector potential $\underline{A}$, [23]:

$$\nabla\times\left(\frac{1}{\mu\left(B\right)}\nabla\times\underline{A}\right)=\begin{cases}\underline{J} & \text{steady state,}\\ \underline{J}-\Omega\sigma_{\mathrm{el}}\underline{A}-\sigma_{\mathrm{el}}\nabla u & \text{transient.}\end{cases} \tag{3}$$

B is the flux density and μ the magnetic permeability. The current density $\underline{J}$ describes the current distribution in an electrical conductor, σ_{el} is the electrical conductivity and u the voltage. The term $\mu\left(B\right)$ allows for taking non-linear, i. e. saturation of ferromagnetic material, into account. For transient analyses, only harmonic problems can be considered in FEMM.

For simulation of a heteropolar magnetic bearing, a planar model can be used. A complete magnetic shielding of the bearing is assumed, i. e. the magnetic vector potential at the outer radius of the stator is 0 (*Dirichlet* boundary condition):

$$\underline{A}\big|_{r=r_{\mathrm{St,a}}}\stackrel{!}{=}\underline{0}. \tag{4}$$

2.2.1 Force Computation

The force acting on the rotor is calculated on the basis of [25] and [26] using the weighted *Maxwell* stress tensor Θ:

$$\underline{F}=-\int_S\Theta\cdot\nabla\varepsilon\mathrm{d}S. \tag{5}$$

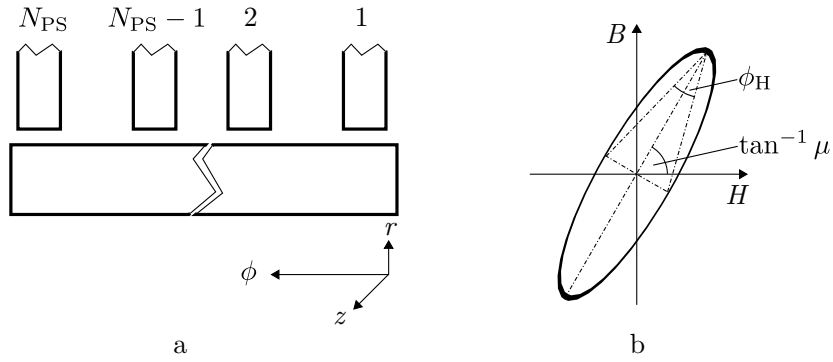

Figure 2: Iron loss model proposed in [27]: "Unrolled" model of the magnetic bearing with N_{PS} pole shoes for showing the periodicity in ϕ (a); Visualization of the complex permeability μ_j (b)

Thereby, the stress tensor is integrated along a thin area S along the rotor surface. The scalar quantity ε includes a weighting function [26].

2.2.2 Loss Computation

The following losses occur in magnetically levitated shafts, [5]:

- eddy current and hysteresis losses, P_{EC} and P_{H} (iron losses P_{Fe}),
- copper losses P_{Cu},
- switching losses/losses of electronic devices, and
- windage losses.

The first three losse types occur in the magnetic bearings as well as in the rotor. Switching losses and losses of electronic devices are neglected in the following. Windage losses are negligible for vacuum applications.

The copper losses P_{Cu} are calculated using an analytical model:

$$P_{\mathrm{Cu}} = R_{\mathrm{Cu}} i_{\mathrm{act}}^2 \text{ with } R_{\mathrm{Cu}} = \rho_{\mathrm{el}} \frac{l_{\mathrm{Cu}}}{A_{\mathrm{Cu}}}, \tag{6}$$

where R_{Cu} is the winding resistance and i_{act} is the actual bearing and motor current, respectively. The winding resistance depends on the specific electrical resistance ρ_{el}, the length l_{Cu} and the cross section A_{Cu} of the wire.

For the iron loss determination of the heteropolar bearings, a semi-analytical approach proposed by *Meeker* and *Maslen* in [28] is used. It bases on the harmonic analysis of a 1D magnetic field computation and has been introduced in [29] for determine the eddy current losses of a transformer. For this approach, it is assumed that the iron sheets are sufficiently thin, i. e. the axial component of the magnetic field can be neglected. For the magnetic bearing problem, *Meeker* and *Maslen* take advantage of the 2π-harmonic behavior of the magnetic field along the rotor surface, see figure 2 a. Hence, the magnetic flux density B can be represented as the sum of the harmonics in ϕ:

$$B = \mathrm{Re}\left(\sum_{k=0}^{\infty} {}^{k}b e^{jk\phi}\right). \tag{7}$$

Therein, ϕ is the angle about the z-Achse and ${}^{k}b$ represents the k^{th} harmonic of B. In [27], hysteresis losses are added by including the complex permeability $\mu_j = \mu e^{-j\phi_{\text{H}}}$, where ϕ_{H} is the hysteresis angle, see figure 2 b. The overall losses can be written as the sum of the losses of each harmonic ${}^{k}P$:

$$P_{\text{Fe}} = \sum_{k=0}^{\infty} {}^{k}P = -\pi\omega k^2 \delta \text{Im}\left({}^{k}\mu\right) \tanh\left[\frac{k}{r_{\text{R,o}}}\left(r_{\text{R,o}} - r_{\text{R,i}}\right)\right] \left|{}^{k}\Phi(r_{\text{R,o}})\right|^2 \tag{8}$$

with the permeability of the k^{th} harmonic

$${}^{k}\mu = \mu_j \frac{\tanh\left(\frac{\delta}{2}\sqrt{jk\omega\sigma_{\text{el}}\mu_j}\right)}{\frac{\delta}{2}\sqrt{jk\omega\sigma_{\text{el}}\mu_j}}, \tag{9}$$

$\Phi(r_{\text{R,o}})$ is the scalar magnetic potential along the outer rotor radius:

$$\left.\frac{\partial\, {}^{k}\Phi}{\partial r}\right|_{\text{R,o}} = \frac{{}^{k}\mu}{\mu_0}\frac{k}{r_{\text{R,o}}} \tanh\left[\frac{k}{r_{\text{R,o}}}\left(r_{\text{R,o}} - r_{\text{R,i}}\right)\right] {}^{k}\Phi(r_{\text{R,o}}). \tag{10}$$

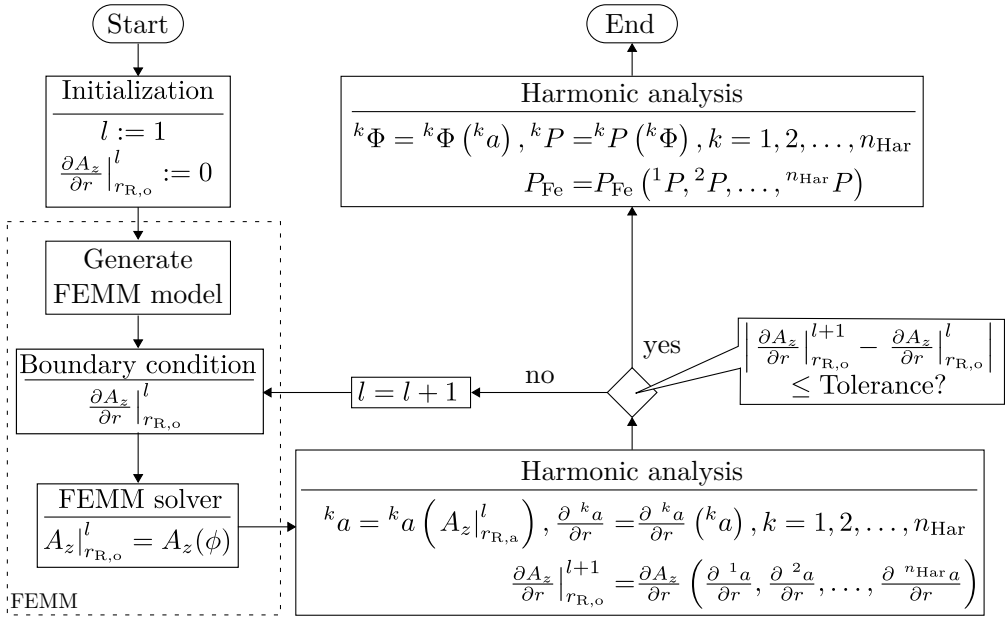

Legend

A_z... Axial component of the magnetic vector potential
${}^{k}a$... k^{th} harmonic of the magnetic vector potential
${}^{k}\Phi$... k^{th} harmonic of the scalar magnetic potential
${}^{k}P$... k^{th} harmonic of the losses
P_{Fe}... Iron losses
r... Radial direction
$r_{\text{R,a}}$... outer rotor radius
ϕ... Angle about z axis
l... Iteration step
n_{Har}... Number of Harmonics

Figure 3: Computation procedure of the algorithm for determination of the iron losses by coupling of MATLAB® and FEMM introduced by [30]

A detailed derivation of the required equations can be found in [28] and [27]. In order to include stray fields and saturation effects, the magnetic field is determined in FEMM. Since FEMM is not feasible for performing harmonic analyses, the finite element analyses is coupled to MATLAB®. The required parameters are exchanged between the two programs via "'OctaveFEMM"'. The implemented algorithm is adapted from [30] and shown in figure 3. The determination of the magnetic field by applying equation 10 to the outer rotor surface is done iteratively. The required transformation between Φ and $\underline{A}$ is given by the definition of the magnetic flux density $\underline{B}$, [12]:

$$\underline{B} = -\mu \nabla \Phi = \nabla \times \underline{A}. \tag{11}$$

The motor drive is carried out using a brushless DC motor. Within the scope of this study, only the occurring hysteresis and copper motor losses are considered using simplified equations. The former is determined by

$$P_{\mathrm{Fe}} = c_{\mathrm{Fe}} \Omega, \tag{12}$$

where c_{Fe} is a constant coefficient. Especially during rotor acceleration, relatively high motor currents i_{M} occur that yield high copper losses, see equation 6. Assuming idealized motor behavior, i. e. $\Omega_{\mathrm{act}} = \Omega_{\mathrm{req}}$, and neglecting the motor inductance, the motor current can be written as

$$i_{\mathrm{M}} = \left(I\dot{\Omega} + \frac{P_{\mathrm{R}}}{\Omega} \right) \frac{1}{K_{\mathrm{M}}} \tag{13}$$

with the moment of inertia I, the rotor losses P_{R} that have to be compensated by the motor drive, and the motor constant K_{M}.

2.3 Closing the Control Loop

Active magnetic bearings are not stable, see negative sign in equation 2. Hence, a controller has to been applied, in order to generate the required bearing forces. The required components are modeled applying the following assumptions:

- analogue signal processing
- sensors and amplifier have PT1 behavior,
- PID controller yields sufficient control quality, and
- current control yields simplified controller algorithms when compared to voltage control.

2.4 Thermal Model

The occurring losses yield heating of the components. This in turn, changes the mechanical, electric and magnetic properties of the system. Thus, thermal analyses of such systems are discussed in various publications [31, 32, 33]. In [6, 34, 5, 7] approaches for calculting the temperature of magnetic bearings are introduced. Those models base on thermal networks.

In order to investigate the temperature distribution inside the shaft, the energy balance in conjunction with the *Fourier* heat conduction law according to [35] is used. The analytical solution of the resulting partial differential equations is rather complex or even not possible [35]. Hence, numerical algorithms are used applying the finite difference method.

Generally, the following heat transport processes occur:

- heat conduction,

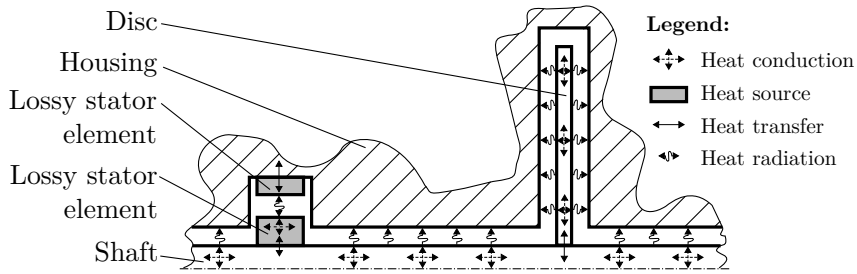

Figure 4: Schematic of the thermal model

- heat radiation, and
- heat convection.

The latter can be neglected when considering vacuum applications. Furthermore, it is assumed that the housing temperatures are constant, i. e. temperature controlled housing. The thermal model is shown schematically in figure 4.

For axially symmetric problems (only radial r and axial z direction considered), the transient temperature field $T(x,t)$ of a volume having the mass density $\rho(T)$, the specific heat capacity $c_p(T)$ and the thermal conductivity $\lambda_{\mathrm{th}}(T)$ can be determined applying the first law of thermodynamics and *Fourier*'s law of heat conduction, [35]:

$$\begin{aligned} &\dot{T}\left(c_p T\frac{\partial \rho}{\partial T}+\rho T\frac{\partial c_p}{\partial T}+\rho c_p\right)=\ldots \\ &\ldots\lambda_{\mathrm{th}}\left(\frac{\partial^2 T}{\partial r^2}+\frac{\partial^2 T}{\partial z^2}\right)+\frac{\partial \lambda_{\mathrm{th}}}{\partial T}\left[\left(\frac{\partial T}{\partial r}\right)^2+\left(\frac{\partial T}{\partial z}\right)^2\right]+\frac{\lambda_{\mathrm{th}}}{r}\frac{\partial T}{\partial r}. \end{aligned} \tag{14}$$

The following boundary conditions are applied:

- *Neumann* (second type) boundary condition for taking external heat sources or adiabatic conditions along the surface of a component into consideration,
- *Robin* (third type) boundary condition for heat transfer between touching components and for heat radiation (the radiated heat can be calculated using the *Stefan-Boltzmann* law, see e. g. [36]).

For the stators of the electromagnetic devices, i. e. magnetic bearings and motor, only a single thermal node including heat transfer to the housing $\dot{Q}_\alpha$, heat radiation exchange between rotor and stator $\dot{Q}_\sigma$, and internal heat sources $\dot{Q}_{\mathrm{in}}$ accounting for stator losses is considered:

$$\frac{\partial}{\partial t}\left(\rho V c_p T\right) \overset{m=const.}{=} \rho V \dot{T}\left(T\frac{\partial c_p}{\partial T}+c_p\right)=\dot{Q}_{\mathrm{in}}-\dot{Q}_\sigma-\dot{Q}_\alpha, \tag{15}$$

where V is the volume and m is the mass, $m=\rho V$, of the stator.

For the numerical solution of the resulting system of equations including the transient temperatures of each considered thermal node, refer to equations 14 and 15, the finite difference method is applied. The spatial discretization results from the central difference quotient yielding a second order accuracy. The time discretization is carried out by the forward difference quotient. This results in an explicit system of equations that can only be solved stably when applying very small step sizes and therewith requiring many computation steps [37]. In order to circumvent this prob-

lem, *Peaceman* and *Rachford* developed the Alternating Direction Implicit method (ADI) yielding general stability [37]. The resulting algorithm solves the system for the time step $m+1$ in radial direction r, i. e. implicitly, and for m in axial direction z, i. e. explicitly. For the next time step $m+2$ the opposite applies – explicit solution in r and implicit solution in z.

For the overall system, the following column vectors for n_r nodes in r direction and n_z nodes in z direction on the shaft and n_{St} lossy stator elements are defined

$$\begin{aligned}
&\text{Shaft temperatures (S): } \underline{T} = (T_{1,1} \;\; T_{2,1} \ldots T_{k,l} \ldots T_{n_r-1,n_z} T_{n_r,n_z})^{\mathrm{T}},\\
&\text{Stator temperatures (St): } \underline{T}_{\mathrm{St}} = (T_{\mathrm{St},1} \;\; T_{\mathrm{St},2} \ldots T_{\mathrm{St},n_{\mathrm{St}}})^{\mathrm{T}} \text{ and}\\
&\text{Housing temperatures (H): } \underline{T}_{\mathrm{H}} = (1 \;\; 1 \ldots 1)^{\mathrm{T}} \cdot T_{\mathrm{H}}.
\end{aligned}$$

Forming the system of differential equations out of each node on the shaft and including the above mentioned boundary conditions, a quartic system of equation for the time 0 results[1]:

$$\begin{aligned}
\underline{0} = {} & (\mathbf{C}_r - \mathbf{C}_c)\,\underline{T}_1 + \mathbf{C}_{\sigma\mathrm{S},r}\underline{T}_1^4 - \mathbf{C}_{\sigma\mathrm{St},r}\underline{T}_{\mathrm{St},1}^4 - \mathbf{C}_{\sigma\mathrm{H},r}\underline{T}_{\mathrm{H}}^4 \ldots\\
\ldots + {} & (\mathbf{C}_z + \mathbf{C}_c)\,\underline{T}_0 + \mathbf{C}_{\sigma\mathrm{S},z}\underline{T}_0^4 - \mathbf{C}_{\sigma\mathrm{St},z}\underline{T}_{\mathrm{St},0}^4 - \mathbf{C}_{\sigma\mathrm{H},z}\underline{T}_{\mathrm{H}}^4 \ldots\\
\ldots + {} & \mathbf{C}_{c2}\left(\underline{T}_0^2 - \mathrm{diag}(\underline{T}_1)\underline{T}_0\right) + \underline{C}_{\dot{q}} \text{ where } \underline{T}_{\mathrm{H}} \in \mathbb{R}^{n_r n_z}.
\end{aligned} \tag{16}$$

For the the time 1, the matrices in r and z have to be changed. The matrices $\mathbf{C}_r$ and $\mathbf{C}_z$ contain the linear terms for heat conduction and transfer. $\mathbf{C}_c$ and $\mathbf{C}_{c2}$ are diagonal matrices that include the heat capacity related terms. Matrices taking account for heat radiation have the index σ. The vector $\underline{C}_{\dot{q}}$ yields the external heat fluxes.

For the lossy stator elements (St), equation 15 yields

$$\begin{aligned}
\underline{0} = {} & -\mathbf{C}_{\mathrm{St},c}\underline{T}_{\mathrm{St},1} + \ldots\\
& \ldots + (\mathbf{C}_{\mathrm{St},c} - \mathbf{C}_{\alpha\mathrm{St}})\,\underline{T}_{\mathrm{St},0} + \mathbf{C}_{\alpha\mathrm{H}}\underline{T}_{\mathrm{H}} - \mathbf{C}_{\sigma\mathrm{St}}\underline{T}_{\mathrm{St},0}^4 + \mathbf{C}_{\sigma\mathrm{S}}\underline{T}_0^4 \ldots\\
& \ldots + \mathbf{C}_{\mathrm{St},c2}\left(\underline{T}_{\mathrm{St},0}^2 - \mathrm{diag}(\underline{T}_{\mathrm{St},1})\underline{T}_{\mathrm{St},0}\right) + \underline{C}_{\dot{Q}} \text{ where } \underline{T}_{\mathrm{H}} \in \mathbb{R}^{n_{\mathrm{St}}}.
\end{aligned} \tag{17}$$

The matrices are defined analogues to equation 16.

Equations 16 and 17 can be solved using the least square method in MATLAB® (function `fsolve()`). Since the rotor and stator temperatures are coupled, both equations are included in an iteration loop.

3 Coupled Algorithm

In order to couple the previously shown models of the rotordynamics, electromagnetism, control loop and thermodynamics, various methods are used as shown in figure 5. The main aspect is the inclusion of the electromagnetic quantities bearing forces and losses via look-up tables (LUT), i.e. $\underline{F}_{\mathrm{B}} = \underline{F}_{\mathrm{B}}(\underline{w}_{\mathrm{B}}, \underline{i}_{\mathrm{act}}, \vartheta, \vartheta_{\mathrm{St}})$ and $P_{\mathrm{Fe}} = P_{\mathrm{Fe}}(\Omega, \underline{i}_{,\mathrm{act}}\, \vartheta, \vartheta_{\mathrm{St}})$. The coupling of the thermal and electromechanical circuit is carried out by updating the system matrices of both circuits for each computation step. In table 1, all considered temperature dependent mechanical, electrical and magnetic parameters of the overall model are shown.

[1] $\underline{T}^n := (T_1^n \;\; T_2^n \ldots)^{\mathrm{T}}$, $n = \{2,\ 4\}$

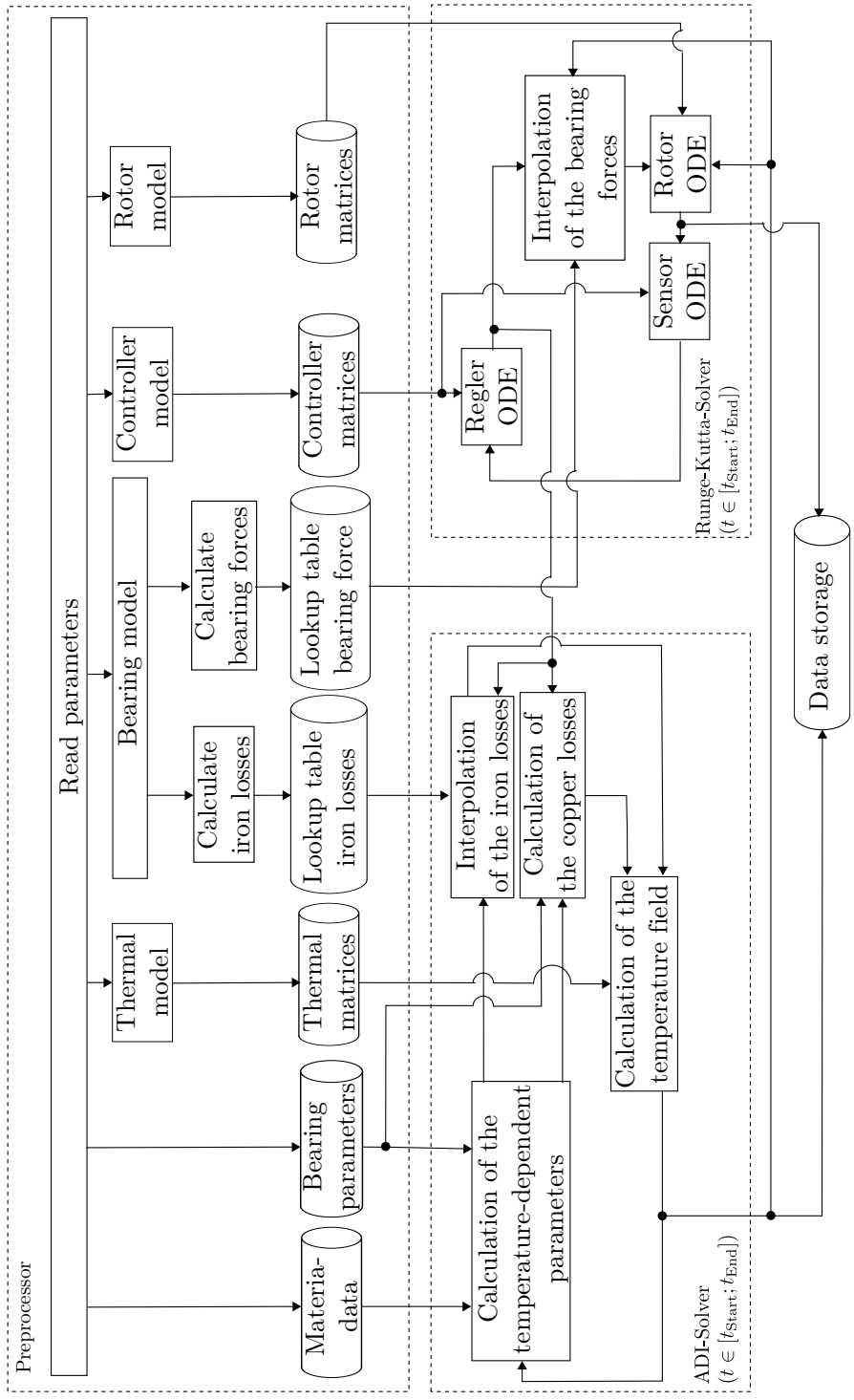

Figure 5: Algorithm of the thermal-electromechanical analysis of a magnetically levitated shaft (ADI. . . Alternating Direction Implicit (Method); ODE. . . Ordinary Differential Equation)

Table 1: Considered temperature dependent parameters

Components	Parameter	Influenced quantities
Shaft	Young's modulus E	Eigenfrequency
Permanent magnets	Remanence B_{R}, coercivity H_{c}	Iron losses Bearing force
Turns	Electrical resistance ρ_{el}	Copper losses
Rotor laminations	Electrical conductivity σ_{el}, rotor radius $r_{\mathrm{R,o}}$	Iron losses Bearing force
Stator laminations	Pole shoe radius r_{PS}	Iron losses Bearing force

4 Example computations

4.1 Example I: Transient Analysis

In the following, a transient coupled analysis is discussed. In figure 6 the considered reference system is shown. The magnetically levitated shaft is accelerated from 0 to 300 Hz with 0.5 Hz/s. The overall simulated time is 8 h, in order to reach a thermal equilibrium.

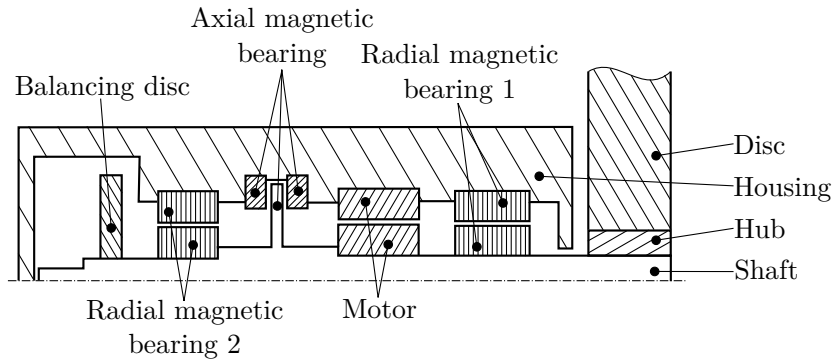

Figure 6: Reference system for the example analysis

In figure 7, the rotor speed and the temperatures of the bearings and motor are plotted. After 10 min the maximum rotor speed is reached. The rotor temperatures increase continuously and reach values between 160 °C and 190 °C. For the stator temperatures, the behavior of the bearings is similar, whereas the motor stator reaches a maximum after approximately 10 min, since the highest losses in the motor stator occur during acceleration of the shaft. It becomes obvious that the time dependent behavior of the losses has a main influence on the temperature characteristics. Hence, the losses are discussed in the following.

The occurring iron losses of the magnetic bearings depend on the rotor speed and the temperatures ϑ_{R} and ϑ_{St}, see figure 8. For the reference system, the losses reach a maximum of 67 W and 94 W at $t \approx 10$ min. After 8 h, the losses are 50 W and 70 W. Hence, even at constant rotor speed the losses decrease by approximately 25 % due to the temperature depedence of the bearing properties.

The copper losses look different. For the magnetic bearings, they increase with increasing temperatures, since the electrical resistance increases as well. For the motor, the copper losses decrease after reaching the maximum speed, since no electrical current is required for accelerating the rotor

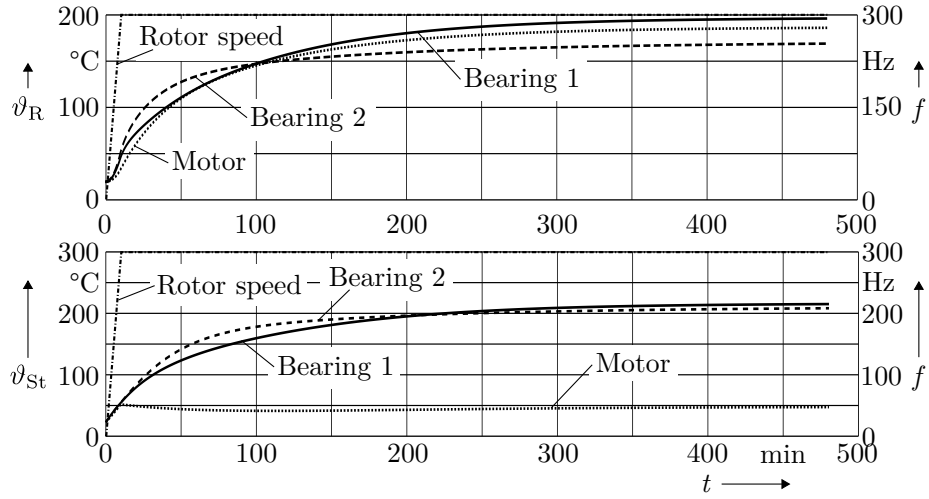

Figure 7: Time dependent behavior of the rotor speed f and the rotor and stator temperatures, ϑ_R and ϑ_{St}, of the bearings and the motor

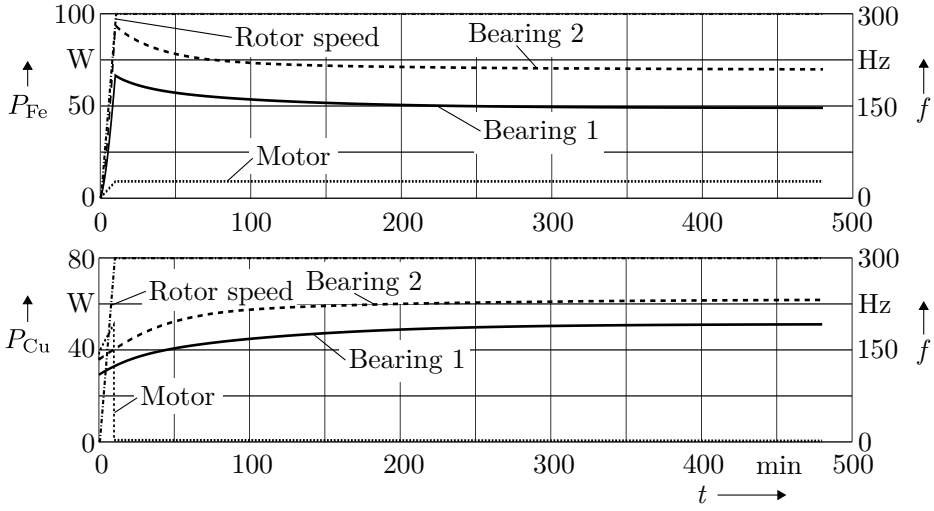

Figure 8: Time dependent behavior of the rotor speed f and the rotor and stator losses, P_{Fe} and P_{Cu}, of the bearings and the motor

after having reached the required operational speed. Only the occurring bearing rotor losses need to be compensated for constant rotor speeds. The previously shown loss characteristics indicate that the magnetic bearing properties will change (drastically) during rotor acceleration. These effects are considered in the following, see figure 9. It becomes obvious that the air gap firstly increases before decreasing and reaching the steady state. This is caused by the difference between rotor and stator temperatures and it also influences the bearing force coefficients.

Since the shaft and bearing properties change during acceleration due to temperature changes, see table 1, there might be critical states that can only be identified when carrying out coupled analyses. In figure 10 a, it is plotted how the bearing air gap changes over rotor speed. It can be seen

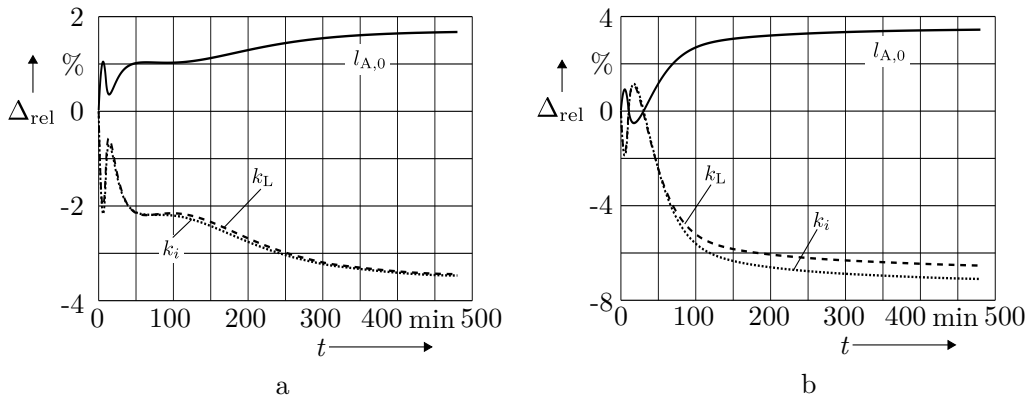

Figure 9: Time dependent behavior of the magnetic bearing properties: relative air gap $l_{\mathrm{A},0}$ and linear force-displacement and force-current coefficient, k_{B} and k_i, change of bearing 1 (a) and bearing 2 (b)

that the gaps reach a maximum between 150 and 175 Hz. Hence, the bearing yield a minimum force at this point. This might lead to insufficient rotor suspension in this rotor speed range. Therefore, the following states will be considered more detailed:

- 0 Hz at 20 °C,
- 175 Hz with maximum air gap, and
- 300 Hz at thermal equilibrium.

It becomes obvious that there is an eigenfrequency at the above mentioned range between 150 and 175 Hz. Nonetheless, the bearing suspension seems to be sufficient for all three stated, since the gyroscopic damping positively influences the bearing force reduction.

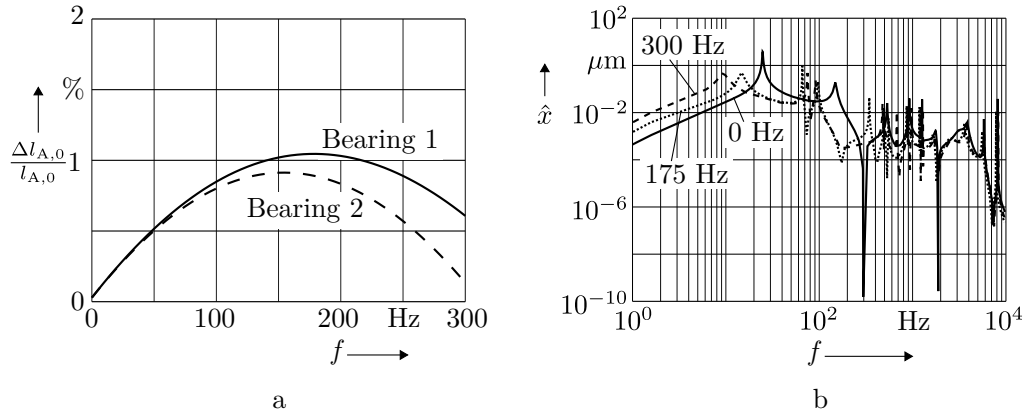

Figure 10: Identification of possible critical states considering the air gap $l_{\mathrm{A},0}$ during acceleration (a) and using the *Bode*-Plot (b)

4.2 Example II: Approach for experimental loss determination using thermal analyses

The thermal model of the magnetically levitated shaft in combination with temperature measurements along the shaft can be used for determine the occurring losses. For that purpose, the steady-state temperatures are correlated with computations. The developed algorithm is shown schematically in figure 11. It bases on combinatory analyses of the physically possible loss values basing on a first estimation of the overall losses P_{tot}.

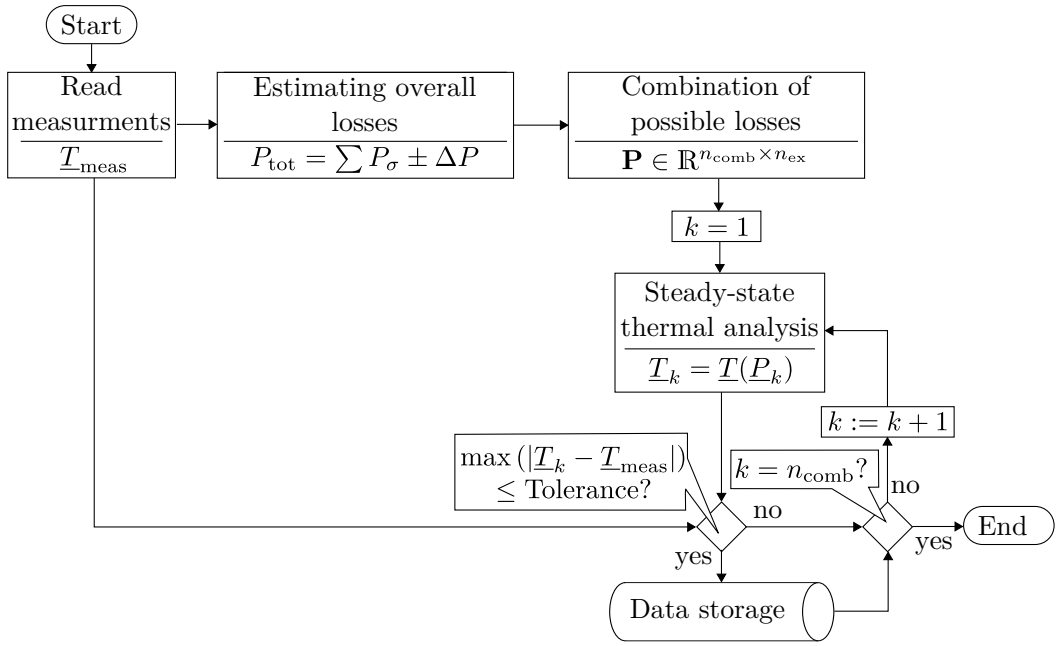

Figure 11: Algorithm for experimental loss determination using thermal analyses

For the reference system shown in figure 6, this approach has been used. The losses are determined at a speed of 21.000 rpm. The temperatures are measured at the following positions: between balancing disc and radial magnetic bearing 2 (sensor 1), between axial bearing and motor (sensor 2), between radial magnetic bearing 1 and disc (sensor 3), and at the disc (Sensor 4). The measured steady state measurements are 71 °C (sensor 1), 75 °C (sensor 2), 79 °C (sensor 3) and 27 °C (sensor 4). The housing temperature was $\vartheta_{\mathrm{H}} = 20\,^{\circ}\mathrm{C}$. These values and the knowledge of the materials and geometries can be used for determine the occurring losses.

For the example analysis, $n_{\mathrm{comb}} \approx 600.000$ have been used to determine the losses. In figure 12, the most probably losses are plotted. It can be seen that the algorithm converges, since all 174 results yield the same general conclusions:

- the losses of bearing 2 are between 38 W and 46 W,
- tho other heat sources are between 0 W and 10 W.

These results are supposed to be very realistic, since bearing 2 is closed to the center of gravity of the shaft and therewith yields high electrical currents. Further analyses of this algorithm should be considered to evaluate the quality of the results. Nonetheless, it has to be again mentioned that the above results have extracted from a number of $n_{\mathrm{comb}} \approx 600.000$ possible combination of losses.

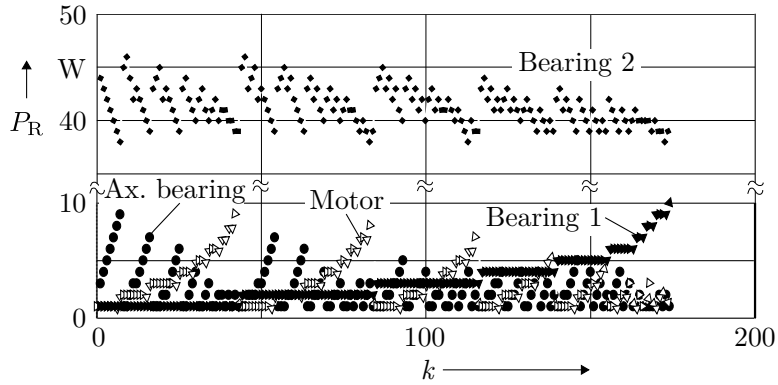

Figure 12: Results of the experimental loss determination using thermal analyses

Hence, the general approach of this analysis is supposed to be a good alternative to rundown tests, especially when investigating systems where the temperature is monitored anyway.

References

[1] M. Ahrens and L. Kučera. Cross feedback control of a magnetic bearing system – controller design considering gyroscopic effects. In *Proceedings of the 3rd International Symposium on Magnetic Suspension Technology*, 1995.

[2] D. Laier. *Nichtlinearitäten magnetgelagerter Rotorsysteme*. PhD thesis, Technische Universität Darmstadt, 1998. ISBN: 3-18-327311-X.

[3] H. Stegemann. *Neuartige Verfahren für die Modellierung und digitale Regelung aktiv magnetgelagerter Systeme*. PhD thesis, Technische Universität Bergakademie Freiberg, 2002.

[4] R. Gasch, R. Nordmann, and H. Pfützner. *Rotordynamik*. Springer-Verlag, 2., vollst. neubearb. u. erw. aufl. edition, 2006. ISBN: 3-540-41240-9.

[5] G. Schweitzer and E. Maslen, editors. *Magnetic Bearings – Theory, Design, and Application to Rotating Machinery*. Springer-Verlag Berlin Heidelberg, 2009. ISBN: 978-3-642-00496-4.

[6] A. Traxler. *Eigenschaften und Auslegung von berührungsfreien elektromagnetischen Lagern*. PhD thesis, Eidgenössische Technische Hochschule Zürich, 1985.

[7] H. Ueyama and M. Taniguchi. Thermal simulation of rotating machine equipped with active magnetic bearings. In *Proceedings of the 12th International Symposium on Magnetic Bearings*, pages II–XI, 2010.

[8] S. R. H. Hoole. *Computer-Aided Analysis and Design of Electromagnetic Devices*. Elsevier Science Publishing Co., Inc., 1989. ISBN: 0-444-01327-X.

[9] S. Blume. *Theorie elektromagnetischer Felder*. Hüthig Buchverlag Heidelberg, 3., überarbeitete auflage edition, 1991. ISBN: 3-7785-2070-9.

[10] H. Frohne. *Elektrische und magnetische Felder*. B. G. Teubner Stuttgart, 1994. ISBN: 3-519-06404-9.

[11] J. Fetzer, M. Haas, and S. Kurz. *Numerische Berechnung elektromagnetischer Felder*. expert verlag, 2002. ISBN: 3-8169-2012-8.

[12] J. D. Jackson. *Klassische Elektrodynamik*. Walter de Gruyter GmbH & Co. KG, Berlin, 4., überarbeitete auflage edition, 2006. ISBN: 3-11-018970-4.

[13] M. Lang. *Berechnung und Optimierung von passiven permanentmagnetischen Lagern für rotierende Maschinen*. PhD thesis, Technische Universität Berlin, 2003. ISBN: 3-18-335721-6.

[14] L. Burdet. *Active Magnetic Bearing Design and Characterization for High Temperature Applications*. PhD thesis, Ecole Polytechnique Federale de Lausanne, 2006.

[15] G. Li, Z. Lin, P.E. Allaire, and J. Luo. Modeling of a high speed rotor test rig with active magnetic bearings. *Journal of Vibration and Acoustics*, 128:269–281, 2006.

[16] S. E. Mushi, Z. Lin, and P. E. Allaire. Stability analysis for a flexible rotor on active magnetic bearings subject to aerodynamic loads. In *Proceedings of the 12th International Symposium on Magnetic Bearings*, pages 1–7, 2010.

[17] T. Dimond, R. Rockwell, G. Simmons, and P. Allaire. Comparison of load capacity and inductance for common active magnetic bearing designs. In *Proceedings of the 12th International Symposium on Magnetic Bearings*, pages 117 – 126, 2010.

[18] R. Larsonneur. *Design and Control of Active Magnetic Bearing Systems for High Speed Rotation*. PhD thesis, Swiss Federal Institue of Technology Zurich, 1990.

[19] T. Roschke. *Entwurf geregelter elektromagnetischer Antriebe für Luftschütze*. PhD thesis, Technische Universität Dresden, 1999. ISBN: 3-18-329321-8.

[20] Tera Analysis Ltd. Quickfield™: Finite element analysis system – version 5.7, 2009. User's Manual.

[21] ANSYS, Inc. Maxwell® 13.0 data sheet, 2010.

[22] CEDRAT Group. Flux® data sheet, 2010.

[23] D. Meeker. Finite element method magnetics – version 4.2, 2007. User's Manual.

[24] Tera Analysis Ltd. Students' quickfield™, 2010.

[25] S. McFee, J. P. Webb, and D. A. Lowther. A tunable volume intergration formulation for force calculation in finite-element based computational magnetostatics. *IEEE Transactions on Magnetics*, 24(1):439–442, 1988.

[26] F. Henrotte, G. Deliege, and K. Hameyer. The eggshell approach for the computation of electromagnetic forces in 2d and 3d. *International Journal for Computation and Mathematics in Electrical and Electronic Engineering*, 23(4):996–1005, 2004.

[27] D. C. Meeker, A. V. Filatov, and E. H. Maslen. Effect of magnetic hysteresis on rotational losses in heteropolar magnetic bearings. *IEEE Transactions on Magnetics*, 40(5):3302 – 3307, 2004.

[28] D. C. Meeker and E. H. Maslen. Prediction of rotating losses in heteropolar radial magnetic bearings. *Journal of Tribology*, 120(3):629 – 635, 1998.

[29] R. L. Stoll. *The analysis of eddy currents*. Clarendon Press, Oxford, 1974.

[30] D. Meeker. Calculation of rotational losses in heteropolar magnetic bearings with femm, 2006.

[31] T. Harriehausen. *Messwertgestützte Simulation der Temperaturverteilung in axial segmentierten Walzen*. PhD thesis, Universität Hannover, 1992.

[32] Y. Huai, R. V.N. Melnik, and P. B. Thogersen. Computational analysis of temperature rise phenomena in electric induction motors. *Applied Thermal Engineering*, 23:779–795, 2003.

[33] Z. Kolondzovski. *Thermal and Mechanical Analyses of high-speed Permanent-Magnet Electrical Machines*. PhD thesis, Aalto University, 2010.

[34] L. Burdet, B. Aeschlimann, and R. Siegwart. Thermal model for a high temperature active magnetic bearing. In *Proceedings of the 9th International Symposium on Magnetic Bearings*, 2004.

[35] H. Martin. Instationäre wärmeleitung in ruhenden körpern. In *VDI-Wärmeatlas*, pages Ec1 – Ec24. Springer-Verlag Berlin Heidelberg, 10. auflage edition, 2006. ISBN: 3-540-25503-6.

[36] J. H. Lienhard IV and J. H. Lienhard V. *A Heat Transfer Text Book*. Phlogiston Press, 3. auflage edition, 2008.

[37] D. W. Peaceman and H. H. Rachford, Jr. The numerical solution of parabolic and elliptic differential equations. *The Numerical Solution of Parabolic and Elliptic Differential Equations*, 3(1):28–41, 1955.